

Characterization of Hall effect thruster propellant distributors with flame visualization

S. Langendorf and M. L. R. Walker

Citation: *Rev. Sci. Instrum.* **84**, 013302 (2013); doi: 10.1063/1.4774049

View online: <http://dx.doi.org/10.1063/1.4774049>

View Table of Contents: <http://rsi.aip.org/resource/1/RSINAK/v84/i1>

Published by the [American Institute of Physics](#).

Related Articles

Emission spectroscopy of the interior of optically dense post-detonation fireballs
[J. Appl. Phys. 113, 024903 \(2013\)](#)

Effect of acoustic coupling on power-law flame acceleration in spherical confinement
[Phys. Fluids 25, 013602 \(2013\)](#)

Two-dimensional direct numerical simulation evaluation of the flame-surface density model for flames developing from an ignition kernel in lean methane/air mixtures under engine conditions
[Phys. Fluids 24, 105108 \(2012\)](#)

Asymptotic structure of laminar diffusion flames at high pressure
[Phys. Fluids 24, 093602 \(2012\)](#)

On the compressible Hart-McClure and Sellars mean flow motions
[Phys. Fluids 24, 096101 \(2012\)](#)

Additional information on Rev. Sci. Instrum.

Journal Homepage: <http://rsi.aip.org>

Journal Information: http://rsi.aip.org/about/about_the_journal

Top downloads: http://rsi.aip.org/features/most_downloaded

Information for Authors: <http://rsi.aip.org/authors>

ADVERTISEMENT



**Does your research require low temperatures? Contact Janis today.
Our engineers will assist you in choosing the best system for your application.**



- 10 mK to 800 K
- LHe/LN₂ Cryostats
- Cryocoolers
- Magnet Systems
- Dilution Refrigerator Systems
- Micro-manipulated Probe Stations

sales@janis.com www.janis.com
Click to view our product web page.

Characterization of Hall effect thruster propellant distributors with flame visualization

S. Langendorf^{a)} and M. L. R. Walker^{a)}

High-Power Electric Propulsion Laboratory, Georgia Institute of Technology, 625 Lambert St. NW, Atlanta, Georgia 30318, USA

(Received 18 June 2012; accepted 16 December 2012; published online 9 January 2013)

A novel method for the characterization and qualification of Hall effect thruster propellant distributors is presented. A quantitative measurement of the azimuthal number density uniformity, a metric which impacts propellant utilization, is obtained from photographs of a premixed flame anchored on the exit plane of the propellant distributor. The technique is demonstrated for three propellant distributors using a propane-air mixture at reservoir pressure of 40 psi (gauge) (377 kPa) exhausting to atmosphere, with volumetric flow rates ranging from 15–145 cfh (7.2–68 l/min) with equivalence ratios from 1.2 to 2.1. The visualization is compared with in-vacuum pressure measurements 1 mm downstream of the distributor exit plane (chamber pressure held below 2.7×10^{-5} Torr-Xe at all flow rates). Both methods indicate a non-uniformity in line with the propellant inlet, supporting the validity of the technique of flow visualization with flame luminosity for propellant distributor characterization. The technique is applied to a propellant distributor with a manufacturing defect in a known location and is able to identify the defect and characterize its impact. The technique is also applied to a distributor with numerous small orifices at the exit plane and is able to resolve the resulting non-uniformity. Luminosity data are collected with a spatial resolution of 48.2–76.1 μm (pixel width). The azimuthal uniformity is characterized in the form of standard deviation of azimuthal luminosities, normalized by the mean azimuthal luminosity. The distributors investigated achieve standard deviations of 0.346 ± 0.0212 , 0.108 ± 0.0178 , and 0.708 ± 0.0230 mean-normalized luminosity units respectively, where a value of 0 corresponds to perfect uniformity and a value of 1 represents a standard deviation equivalent to the mean. © 2013 American Institute of Physics. [<http://dx.doi.org/10.1063/1.4774049>]

I. INTRODUCTION

A. Neutral propellant flow in Hall effect thrusters

The Hall effect thruster (HET) is a promising type of electric propulsion device for spacecraft and has accumulated a substantial flight record on many governmental space agency missions and more recently on commercial satellites. HETs deliver substantial propellant mass savings over chemical propulsion for in-space maneuvering by accelerating propellant gas with external energy to increase exhaust velocity and specific impulse.¹ HETs do not depend on chemical energy stored within reactive propellant mixtures, thus they are said to be power-limited rather than energy-limited, with their main performance barriers (low thrust and need for external power source/power processing) being technological rather than physical in nature.

The HET operates by ionizing neutral atoms of propellant gas by collisions with electrons supplied from an external cathode and accelerating those ionized atoms using an axial electric field. The atoms are injected into an annular discharge chamber through a conductive propellant distributor, which fulfills two functions in HET operation: (1) it is the injection path through which the propellant gas is supplied, and (2) it is the anode in the thruster electrical circuit. A radial magnetic field magnetizes the electrons in order to impede their mobility to the anode/propellant distributor and

increase their residence time in the discharge chamber, where they can collide with and ionize injected neutral propellant atoms. The terms “anode” and “propellant distributor” both refer to the same thruster component; in this article the term “propellant distributor” will be used.

The neutral propellant flow parameters of a HET that are of greatest interest are those correlated with thruster performance, lifetime, and operational stability. One of these parameters is the azimuthal uniformity of the number density at the propellant distributor exit plane, which is correlated with thruster electrical efficiency.^{2,3} The importance of this parameter stems from the aforementioned fact that a HET gas distributor also acts as the anode in the thruster electric circuit—any localized increase in mass flux at the distributor exit plane will result in a localized increase in plasma density and increased electron mobility to the anode. This increase in discharge current increases the thruster power draw, and thus represents a direct decrease in thruster efficiency. A mechanism theorized for this increased mobility is that as a local concentration of electrons generated become magnetized and begin their $E \times B$ drift around the discharge chamber annulus, they give rise to a localized azimuthal electric field which interacts with the radial magnetic field to cause another $E \times B$ drift of these electrons towards the anode. Instabilities, plume asymmetries, and decreased thruster efficiency have been observed when azimuthal uniformity is compromised by a defect.⁴ Thus, there is a need to improve the azimuthal uniformity of injected neutrals at the propellant distributor exit plane in order to further increase thruster efficiency. The

^{a)}Also at Department of Aerospace Engineering, Georgia Institute of Technology, 270 Ferst Dr. NW, Atlanta, Georgia 30332-0150, USA.

development of a quantitative and high-resolution measurement of azimuthal number density uniformity is the main objective of this effort.

B. HET neutral flow diagnostics

Current quantitative methods employed to study HET propellant distributor flow are divided into two categories: (1) techniques that employ a physical probe positioned in the downstream flow and (2) non-intrusive optical techniques. Physical probes include pressure transducers and Pitot tubes with dimensions and measurement ranges suitable for HET discharge channel conditions (1–10 mTorr, transitional flow³) and desired spatial resolution. Non-intrusive methods include diagnostics such as laser-induced fluorescence (LIF)^{5,6} and electron-induced fluorescence.⁷ Intrusive methods have intrinsic disadvantages. The spatial resolution of a transducer measurement can be no less than the physical dimensions of its interface to the plasma, usually an inlet tube. Decreasing the diameter of this inlet tube does increase spatial resolution, but also increases the measurement settling time as well the impact of boundary layer formation in the inlet tube.⁸ In addition, there is need for a motion system with positional accuracy and repeatability of the desired spatial resolution. As such, probe measurements are limited in their ability to resolve details of the neutral flux uniformity.

LIF is a non-intrusive diagnostic used to measure neutral velocity, with the advantage that measurements are taken as the thruster operates. However, the requisite 2D optical access is unavailable at locations within the discharge channel. Vial *et al.*⁷ use electron-induced fluorescence to characterize the xenon ion number density inside the channel, gaining optical access through a slot machined along the side. However, the ion density may not mirror the neutral density, and optical access is still unavailable near to the distributor exit plane due to obstruction by the front plate of the magnetic circuit.

Ideal spatial resolution for an azimuthal number density uniformity diagnostic is on the order of the Debye length of the thruster plasma. The Debye length is the length scale of fundamental charge separation in a plasma—for any azimuthal electric field to cause enhancement in electron transport, it must manifest itself at a greater length scale than the Debye length. Typical minimum Debye lengths in HETs are on the order of 10–100 μm .^{9,10} Ideal temporal resolution for an azimuthal number density uniformity diagnostic is determined by the frequency of fluctuations that may affect electron transport and thruster performance. An instability termed the breathing mode has been identified at ~ 20 kHz, though oscillations have been observed at frequencies up to 20 GHz.¹¹ These oscillations are believed to be associated with the plasma rather than the neutral flow characteristics, and consequently the current investigation focuses on spatial resolution.

II. THEORY: FLOW VISUALIZATION BY FLAME LUMINOSITY

In order to quantify the azimuthal uniformity of the neutral number density of HET propellant distributors near their

exit plane, the current effort examines the luminosity of premixed flames located at the propellant distributor exit plane. This technique (hereafter referred to as “flame visualization”) yields a visual representation of the flow at the distributor exit plane which is used to quantify azimuthal uniformity of propellant number density. This method also renders visible any blockages or defects in the unit. The flame is photographed and the azimuthal variation in luminosity recorded. Luminosity is a close follower of mass flux in a premixed near-stoichiometric flame; there is minimal soot formation in comparison to a diffusion flame¹² and thus the luminosity present is caused by excited radicals that relax to more stable states and release photons. As such, if there is a systematic non-uniformity in the flow through the propellant distributor, more excited molecules will be present in the flame regions of higher mass flux and thus more luminosity will be observed in those regions. Because the spatial resolution of flame visualizations is determined by the pixel density of the camera, sub-millimeter spatial resolution is achievable (a 150 mm diameter propellant distributor photographed with a 12 megapixel camera at 4200×2800 would have a pixel width of $53.4 \mu\text{m}$).

A. Applicability

The illustrative flame sheets desired for visualization of the neutral number density cannot be sustained in the rarefied (~ 10 mTorr) exhaust environment required for HET operation,³ so the flame is ignited and photographed at sea level conditions. While this is a convenience in that it removes the need for extensive vacuum test equipment, it raises the question of the applicability and portability of sea level flame visualizations to rarefied HET operating conditions. The perturbing effects of the introduction of the combustion phenomenon must also be assessed.

1. Exhaust environment

For the concern of the atmospheric exhaust environment, Reid’s findings³ indicate that a HET propellant flow is well-modeled by continuum analysis from distributor inlet through distributor exit plane. The dominant feature of this compressible flow is the sonic choked flow that occurs at the smallest orifices in the flow path of the propellant distributor in question. This choked flow is ensured by the ratio of reservoir to exhaust pressure according to Eq. (1), in which P_E is the pressure at the exit of the distributor, P_0 is the supply reservoir pressure, and γ is the gas specific heat ratio. Equation (1) assumes a thermally and calorically perfect gas, which is a reasonable assumption at all operating pressures (≤ 40 psi (gauge)) and temperatures (~ 290 K) in this article,

$$P_E/P_0 = (2/(\gamma + 1))^{\gamma/(\gamma-1)}. \quad (1)$$

In order to ensure that choked flow is reproduced in the flame visualization with atmospheric exhaust pressure, a reservoir pressure > 12.8 psi (gauge) is required as indicated by the solution of Eq. (1) with $\gamma = 1.37$ for a stoichiometric propane-air mixture. A reservoir pressure of 14.7 psi

(gauge) matches the magnitude of the pressure drop that is seen in thruster operation, although for the propellant distributors used in the current study it yields an exit velocity that is insufficient to anchor the flame where it is visible above the distributor exit plane. Consequently, the reservoir pressure is increased to 40 psi (gauge) for the current visualizations. The molecular collision frequency is greater in these atmospheric pressure measurements than in actual thruster operation, and thus the increased collision rate will act to increase density uniformity in atmospheric pressure measurements. However, for the distributor geometries studied, 40 psi (gauge) reservoir pressure yields a much higher flow rate than typical of electric propulsion devices, which increases the magnitude of flow non-uniformities. In light of the high flow rate required, the flame visualization typically amplifies flow non-uniformities, which is eminently desirable in a diagnostic.

2. Combustion effects

The anchoring behavior of flames on the various geometries of thruster propellant distributors complicates efforts to take photographs of diagnostic merit. A premixed flame is able to anchor on an obstruction such as a propellant distributor when two conditions are met: (1) the local flow velocity magnitude is reduced below the laminar flame speed, which occurs near to the stagnation points of the flow provided by the viscous no-slip condition, and (2) the obstruction is able to transfer enough heat away from the adjacent gas to quench the flame at the wall. Thus, it is important to consider the locations at which the flame will anchor on a candidate propellant distributor and to record the flame from a position such that the anchoring locations will not amplify luminosity recorded at any azimuthal location. For this reason, images recorded for analysis are taken from a head-on axial view.

Flames heat their products, and this heating is achieved with negligible pressure drop in the case of a sea level pressure flame. As such, the density of the gas is decreased according to the ideal gas equation of state, introducing a buoyancy perturbation as the light burned gases are impelled upwards. This perturbation is accounted for by photographing the flame from above, so that buoyancy effects will be equivalent at all azimuthal positions.

B. Combustion parameters

The introduction of the combustion phenomenon into a flow diagnostic carries with it the need to ensure that the propellant distributor is not damaged by the sustained heat release of combustion. Choice of gas mixture and equivalence ratio control the peak temperature of combustion, and together with the rate of heat transfer away from the propellant distributor govern the steady-state temperature. If the propellant distributor approaches its melting point, it will begin to glow the characteristic orange of heated metal, indicating that steps should be taken to decrease the steady-state temperature. Propane and air are selected for use as fuel and oxidizer in this experiment. A propane-air flame yields a moderate adiabatic combustion temperature of 2270 K and has a peak laminar

flame speed of 40 cm/s,¹³ with quenching diameter not lower than 1.5 mm.¹⁴

The proportions of propane and air can be varied to create different types of flames, and are reported here in terms of equivalence ratio. Equivalence ratio (ϕ) is a normalized measure of the ratio of fuel to oxidizer in the flame, and is defined in Eq. (2), in which Q_{fuel} = fuel volumetric flow rate, Q_{ox} = oxidizer volumetric flow rate, and the subscript “stoich” indicates the stoichiometric proportions of fuel and oxidizer. For propane-air combustion, these proportions (corresponding to an equivalence ratio of 1) are found by balancing the nominal chemical reaction, Equation (3):

$$\phi = (Q_{fuel}/Q_{ox})/(Q_{fuel}/Q_{ox})_{stoich}, \quad (2)$$



Many of the photographs presented in this article are taken at fuel-rich operating conditions ($\phi > 1$) as the inner flame sheets of the rich flame are found to be very illustrative of the flow distribution, as exemplified in the current study of a propellant distributor with a manufacturing defect. However, the diffuse secondary flame present at rich conditions introduces background luminosity which acts as noise when recording luminosity of the primary flame.

C. Quantification of flow uniformity

In order to obtain a quantitative metric of mass flux uniformity, recorded images are analyzed to compute the normalized azimuthal standard deviation of the luminosity. A recorded exposure (uncompressed JPEG format) contains three values ranging from 0 to 255 for each pixel in the frame. These values are added together to generate a discrete luminosity value for each pixel ranging from 0 to 765, leading to a luminosity resolution of 766 levels between pitch black and pure white. These luminosity values are summed over the radial direction to give a value for each azimuthal position on the propellant distributor, according to Eq. (4), in which L_θ = the luminosity of the radial slice at azimuthal position θ , $L_{r,\theta}$ = the luminosity value of the pixel located at (r, θ) . These L_θ values are normalized by their mean according to Eq. (5), in which \bar{L} = the mean of the L_θ values, and n = the number of azimuthal positions analyzed. In this article, $n = 2400$,

$$L_\theta = \sum_0^R L_{r,\theta}, \quad (4)$$

$$\bar{L} = \frac{1}{n} \sum^n L_\theta. \quad (5)$$

Luminosity values below a threshold are treated as background luminosity and omitted from the summation in Eq. (4). These threshold values are chosen individually for each distributor. A metric σ indicative of the overall azimuthal uniformity is then obtained by computation of the standard deviation of L_θ/\bar{L} .

The discretization of the luminosity data to 766 values causes an uncertainty of $\pm 1/766 = 0.13\%$ full scale, however repeated photographs show greater variation due to flame

fluctuations. Multiple photographs of the flame (eight in this experiment) are processed, and the uncertainty in σ is calculated as the mean deviation of σ of each photograph from the mean σ . This uncertainty is reported separately for each visualization.

III. EXPERIMENTAL SETUP I: FLOW VISUALIZATION BY FLAME LUMINOSITY

Figure 1 shows a flow diagram of the propellant distributor flame visualization setup.

Fuel and oxidizer flow through stainless steel tubing (6.4 mm o.d., 4.1 mm i.d.) through separate 100 psi (gauge) full scale dial pressure gauges and Dwyer RMB-[49-54]-SSV control valve rotameters. The lines are then run 1 m to the propellant distributor, which is mounted facing vertically upward on a frame constructed of 9.5 mm aluminum plate supported by steel strut channel. The fuel and air flows are mixed 0.3 m upstream of the propellant distributor using a pipe tee. The propellant distributor is leveled using a spirit level, yielding a horizontal accuracy of 0.1° . The flame is photographed using a Nikon D90 camera and Nikon AF-S Nikkor 18–105 mm f/3.5-5.6G ED VR lens. The camera is positioned directly above the distributor by using a telescoping tripod that attaches to the camera base as a horizontal mounting arm, keeping the camera at least 1 m above the distributor. Uncertainty in reading the pressure gauges is ± 1 psi, and their accuracy is $\pm 2\%$ mid-scale = ± 1 psi. Uncertainty in reading the rotameters is 2% full scale. They are factory-calibrated for air with accuracy $\pm 3\%$ full scale and corrected for pressure and specific gravity according to Eq. (6), in which Q = corrected volumetric flow rate, Q_{meas} = measured flow rate, P_0 = pressure at upstream side of rotameter, P_{atm} = atmospheric pressure, $\rho_{atm,air}$ = density of air at standard conditions (530 R, 1 atm), $\rho_{atm,gas}$ = density of the flowing gas at

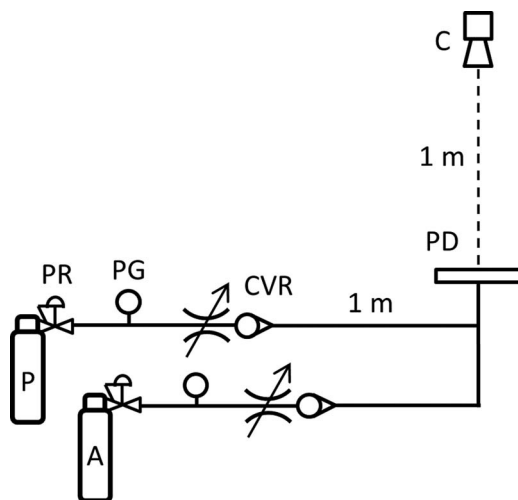


FIG. 1. Schematic of the gas flow feed system and camera for propellant distributor flame visualizations. P = propane cylinder, A = air cylinder, PR = pressure regulator, PG = pressure gauge, CVR = control valve/rotameter, PD = propellant distributor, C = camera.

standard conditions (530 R, 1 atm),

$$Q = Q_{meas} * \sqrt{(P_0 + P_{atm}) / P_{atm}} * \sqrt{(\rho_{atm,air}) / \rho_{atm,gas}} \quad (6)$$

The flame is ignited by using a handheld utility lighter as a pilot flame and operating the control valve to allow a small amount of fuel to flow. To reach desired operating conditions, flow rates of fuel and air are gradually increased using the control valves. For a given operating condition, the temperature of the distributor increases until it reaches a steady state. During this heating, no significant change in the luminosity is measured.

IV. EXPERIMENTAL SETUP II: IN-VACUUM NEUTRAL PRESSURE MEASUREMENT

In order to validate the flame visualization technique as an effective way to characterize azimuthal uniformity of propellant at thruster operating conditions, in-vacuum pressure measurements are obtained near the distributor exit plane using the technique of Reid.³ Figure 2 illustrates the experimental setup.

Xenon is used as working at gas at flow rates of 5, 10, 20, and 40 mg/s. Testing is conducted in HPEPL VTF-2,¹⁵ at pressures from 2×10^{-9} Torr base pressure to 2.7×10^{-5} Torr-Xe at highest flow rate. Vacuum chamber pressure is measured using a Varian 571 ionization gauge and XGS-600 controller, corrected for Xenon by multiplying the indicated pressure by 0.34 as recommended in the XGS-600 user manual. An MKS Baratron 626B capacitance manometer with full scale range 0.1 Torr is used to obtain direct pressure measurements. The sensor is connected via mini-CF flange to a $\frac{1}{4}$ in. stainless steel 90° elbow inlet tube, as shown in Figure 2(b). The tube i.d. is 4.1 mm, and the tube 6.4 mm o.d. is chamfered 45° at the inlet to minimize perturbation of the flow. The inlet tube is positioned at axial distances of 1 mm–2.5 mm downstream from a central radial location on the distributor, which is center-mounted on a rotation stage and turned to measure

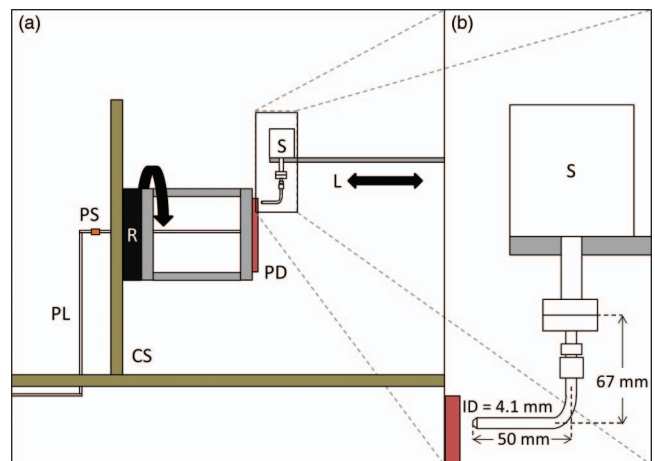


FIG. 2. (a) Diagram of neutral pressure experiment. PL = propellant line, PS = pipe swivel, R = rotation stage, CS = chamber structure, PD = propellant distributor, S = pressure sensor, L = linear motion stage. (b) Detail view of pressure sensor inlet tube.

neutral pressure at different azimuthal locations as shown in Figure 2(a). The propellant line is connected to a pipe swivel and run through the center of the rotation stage. Settling time for the measurement is observed to be approximately 1 second at each azimuthal position; consequently 1.5 s are allowed before collecting data. It is confirmed that the signal from the pressure sensor increases with increasing flow rate, and decreases as it is traversed away from the propellant distributor while gas flow is on.

Uncertainty in axial position of inlet tube is ± 0.1 mm. Uncertainty in radial position of inlet tube is ± 0.2 mm. The accuracy of the capacitance manometer is $\pm 0.25\%$ of reading. A sensor zero-drift of less than 1% signal is observed and is fit and corrected for in data reduction. The highest overall uncertainty of the pressure measurements is $\pm 1\%$ of signal.

V. RESULTS AND DISCUSSION

A. Agreement with in-vacuum pressure measurements

Flame visualization of a propellant distributor with a porous exit plane (Figure 3) revealed a non-uniformity located above the propellant post. Figure 4 shows neutral pressure measurements of the distributor at 1 mm axial distance (2.5 mm axial distance was also studied yielding very similar profiles, so only data at 1 mm are presented). In Figure 5 mean-normalized data from the two techniques are plotted for comparison (normalizing by the mean collapsed all in-vacuum flow rates onto highly similar curves, so only the 5 mg/s case is plotted). Both the visualization and the pressure measurements record a significant peak at 0 rad, corresponding to the location of the single propellant inlet tube to the distributor. This agreement constitutes strong support for the portability of flame visualization luminosity to flow behavior at final operating conditions. The peak has a greater magni-

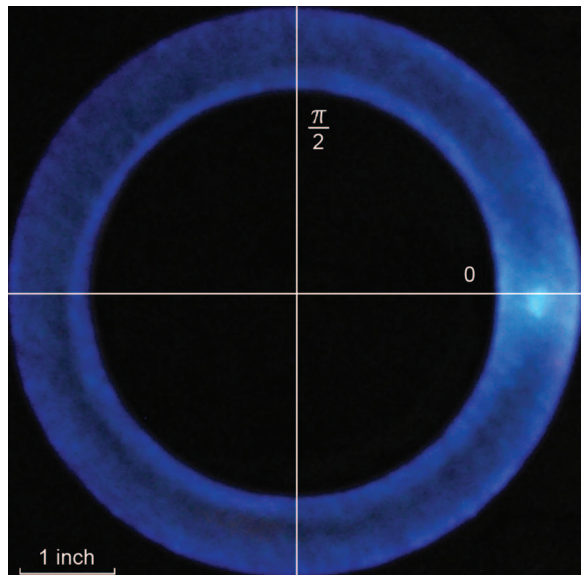


FIG. 3. Flame visualization of propellant distributor with porous exit plane: top view, 40 ± 1.8 psi (gauge), 137 ± 3.9 cfh, $\Phi = 1.7 \pm 0.2$, pixel width of $76.1 \mu\text{m}$.

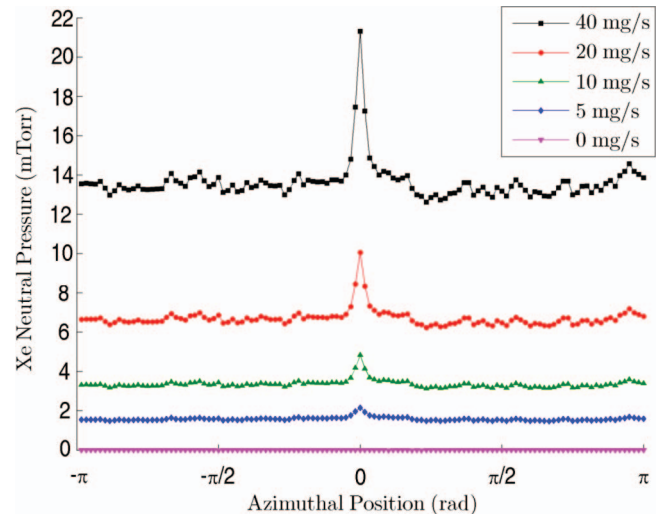


FIG. 4. Measurements of xenon neutral pressure 1 mm downstream of porous propellant distributor exit plane: at 0 mg/s, 5 mg/s, 10 mg/s, 20 mg/s, and 40 mg/s flow rate. Measurement uncertainty $\pm 1\%$ signal, chamber background pressure always $\leq 2.7 \times 10^{-5}$ Torr-Xe.

tude in the flame visualization due to the greatly increased flow rate. This sensitivity is desirable for a diagnostic, in that if one can get the luminosity uniform, the final propellant flow will be extremely uniform.

B. Identification of known manufacturing defect

A propellant distributor with a manufacturing defect along the inner radial propellant distribution pathway is characterized using flame visualization. The study is partially blind in that the experimenters are told the location of the defect, but not its nature or degree of severity. The defect is made visible by the primary flame sheet at a rich operating

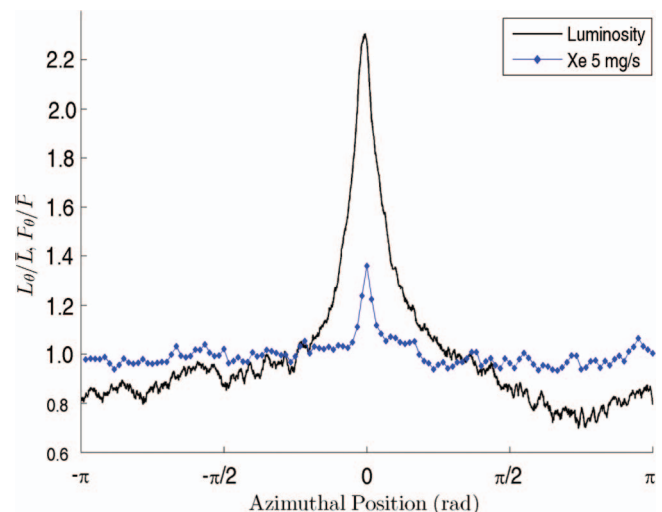


FIG. 5. Comparison of flame visualization and xenon neutral pressure measurements of porous propellant distributor. The data sets are normalized using their respective mean values, as demonstrated in Eq. (5). Background luminosity threshold = 120 luminosity units, luminosity standard deviation $\sigma = 0.346 \pm 0.0212$ mean-normalized luminosity units. Pressure measurements recorded at axial distance 1 mm from distributor exit plane.

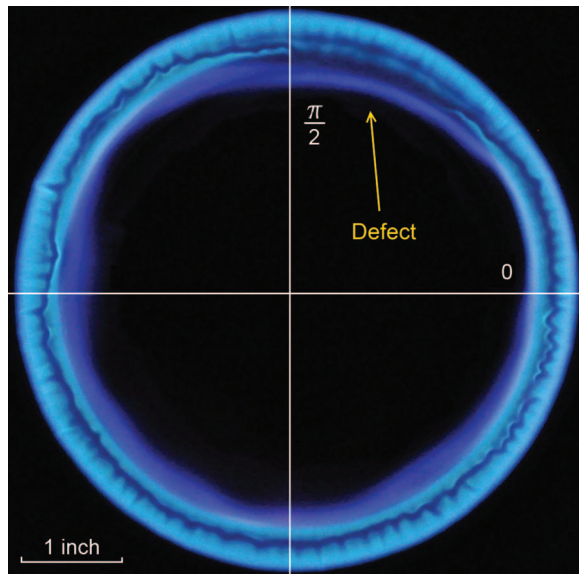


FIG. 6. Flame visualization of propellant distributor with defect: top view, 40 ± 1.8 psi (gauge), 145 ± 4.1 cfh, $\Phi = 1.6 \pm 0.2$, pixel width = $66.3 \mu\text{m}$. Known location of defect indicated.

condition (Figure 6). The identification of this defect affirms the sensitivity of the flame visualization technique (Figure 7). The defect was not apparent for all operating conditions, but became visible at 145 cfh and equivalence ratio 1.6, conditions at which the primary flame is visibly anchored on the exit plane but not lengthened to the point where it washes out luminosity variations. Using the control valves to sweep through a variety of flow rates and equivalence ratios allows the examiner to identify conditions where non-uniformity is most apparent and take photographs at those conditions.

C. Resolution of flow from small inlet orifices

Flame visualization is used to characterize the a HET propellant distributor that differs from the others investigated

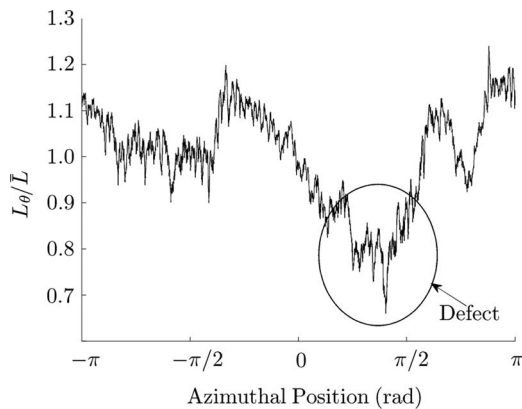


FIG. 7. Flame visualization of propellant distributor with defect, azimuthal luminosity values normalized by mean level using Eqs. (4) and (5). Background luminosity threshold = 220 luminosity units, luminosity standard deviation $\sigma = 0.108 \pm 0.0178$ mean-normalized luminosity units. Defect indicated.

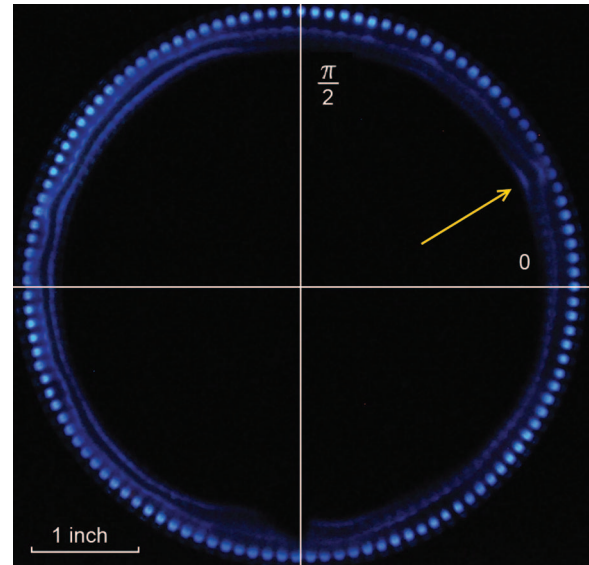


FIG. 8. Flame visualization of propellant distributor with distributed orifices: top view, 40 ± 1.8 psi (gauge), 15.4 ± 0.53 cfh, $\Phi = 1.3 \pm 0.2$, pixel width = $48.2 \mu\text{m}$. Arrow indicates the location of a reduction in propellant flow.

in that the distributor exit plane uses an array of small holes to distribute the working fluid rather than continuous gaps (Figure 8). This results in peaks and valleys in luminosity at each hole and a higher normalized luminosity standard deviation than the other two distributors: $\sigma = 0.748 \pm 0.0230$ mean-normalized luminosity units (Figure 9). It also yields a substantially lower flow rate (15.4 ± 0.53 cfh) than the other distributors at the same reservoir pressure (40 psi (gauge)).

There are 120 peaks and 120 valleys in the luminosity data of Figure 9, as a result of the flow issuing from the 120 small holes around the distributor exit plane. This result highlights the spatial resolution of the technique, showing that it is able to resolve the variations caused by small orifices (0.64 mm diameter) at the distributor exit plane. The visualization also indicates a decrease in flow near $\pi/4$ rad, perhaps corresponding to some blockage or imperfection in the unit.

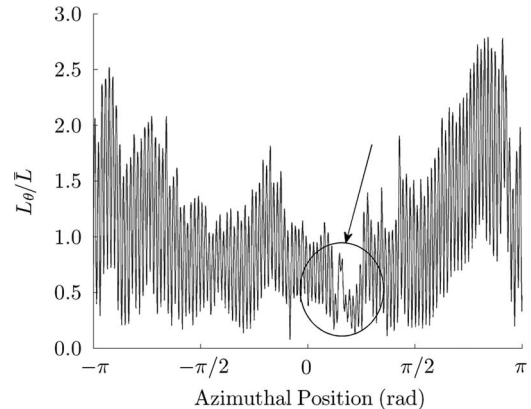


FIG. 9. Flame visualization of propellant distributor with distributed orifices, azimuthal luminosity values normalized by mean level using Eqs. (4) and (5). Background luminosity threshold = 150 luminosity units, luminosity standard deviation $\sigma = 0.748 \pm 0.0230$ mean-normalized luminosity units. Arrow indicates the location of a reduction in propellant flow.

D. Recommendations

The visualizations above have shown the validity and portability of the technique. It has been shown that flame visualizations can be used to identify manufacturing defects, however the relation of defect size to luminosity perturbation was not studied in the current experiment. If making extensive use of the technique in this capacity, this relation could be established after finding several defects.

Flame visualizations could also be used to compare distributors of different design in order to determine which produces the most uniform flow. The current visualizations were performed at different flow rates and equivalence ratios chosen to reveal the greatest possible non-uniformity in each case, which is a concern if trying to use these measurements to compare the three distributors. The measurements are normalized by the mean luminosity value, which may permit comparison between the distributors, however work has not been done to guarantee that such a comparison will accurately represent in-vacuum operation. For rigorous comparisons of visualizations between distributors, it is recommended that they be run at the same equivalence ratio and flow rate. It may not be possible to run all distributors at the same flow rate, as it is necessary to use a flow rate within the range of flow rates that will anchor the flame above the distributor, which is in general different for different geometries. In this case a correction should be devised to account for the differing flow rates.

E. Limitations

With the guidance of flame visualizations, improvements in propellant distributor uniformity could be measured up to the current uncertainty of the technique, which varies but is about ± 0.02 mean-normalized luminosity units. This uncertainty could potentially be further decreased through methods to minimize fluctuations in the flame, such as screens against ambient air currents. Furthermore, the flame luminosity is not able to provide information about the region just adjacent to the propellant distributor (one half the flame quenching diameter¹⁶) because a flame will be locally quenched at the wall and thus will not illuminate that region. In addition, the addition of a thermocouple and readout to the stand would help to determine when a steady-state temperature is achieved as well as aid in the avoidance of dangerous temperatures.

VI. CONCLUSIONS

The flame visualization technique is a novel means of characterizing the neutral flow uniformity of HET propellant distributors. The technique does not require vacuum chamber time or a rotation stage, yet is shown to reproduce the same features seen in vacuum neutral pressure measurements. The technique is also shown to be able to identify manufacturing

defects in HET propellant distributors. It provides greatly improved spatial resolution over what can be achieved with traditional pressure probes, and can be run at high flow rates to amplify and identify flow non-uniformities. As a consequence of these advantages, the flame visualization technique may be a useful tool for HET designers and manufacturers seeking to improve thruster performance and/or thruster qualification processes.

ACKNOWLEDGMENTS

The authors would like to thank Aerojet and Pratt & Whitney Rocketdyne for providing the propellant distributors for these experiments.

The authors would like to thank Graduate Research Assistant Rafael Martinez and Undergraduate Research Assistants Chase Brown and Louis Dressel of GT HPEPL for their assistance in these efforts as well as Graduate Research Assistant Chiluwata Lungu, Graduate Research Assistant Subbiah Ramasamy, Senior Research Engineer David Scarborough, and Research Engineer David Noble of the GT Ben T. Zinn Combustion Laboratory for their consultation and support.

- ¹E. Y. Choueiri, A. J. Kelly, and R. G. Jahn, *AIP Conf. Proc.* **271**, 1187 (1993).
- ²V. Baranov, Y. Nazarenko, and V. Petrosov, in *Proceedings of 27th International Electric Propulsion Conference*, Pasadena, CA, 14–19 October 2001.
- ³B. M. Reid, Ph.D. dissertation, University of Michigan, Ann Arbor, MI, 2009.
- ⁴R. R. Hofer, Ph.D. dissertation, University of Michigan, Ann Arbor, MI, 2004.
- ⁵W. A. Hargus and M. A. Cappell, *Appl. Phys. B* **72**, 961–969 (2001).
- ⁶W. A. Hargus, AIAA Paper 2005-4400, 2005.
- ⁷V. Vial, A. Lazurenko, C. Laure, and A. Bouchoule, in *Proceedings of 28th International Electric Propulsion Conference*, Toulouse, France, 17–21 March 2003.
- ⁸B. Bottin, O. Chazot, M. Carbonaro, V. Van der Haegen, and S. Paris, in *Measurement Techniques for High Temperature and Plasma Flows*, edited by J. M. Charbonnier and G. S. R. Sarma (von Karman Institute for Fluid Dynamics, 1999), NATO-RTO-EN 8.
- ⁹D. M. Goebel and I. Katz, *Fundamentals of Electric Propulsion: Ion and Hall Thrusters*, JPL Space Science and Technology Series (John Wiley & Sons, March 2008) p. 359.
- ¹⁰C. S. Niemala, L. Breida, M. R. Nakles, J. M. Ekholm, and W. A. Hargus, Jr., in *Proceedings of 42nd AIAA/ASME/SAE/ASEE Joint Propulsion Conference and Exhibition*, Sacramento, CA, 9–12 July 2006.
- ¹¹R. B. Lobbia, Ph.D. dissertation, University of Michigan, Ann Arbor, MI, 2010.
- ¹²K. B. Lee, M. W. Thring, and J. M. Beér, *Combust. Flame* **6**, 137–145 (1962).
- ¹³C. M. Vagelopoulos and F. N. Egofoopoulos, *Proc. Combust. Inst.* **27**, 513 (1998).
- ¹⁴C. R. Ferguson and J. C. Keck, *Combust. Flame* **28**, 197–205 (1977).
- ¹⁵A. W. Kieckhafer and M. L. R. Walker, in *Proceedings of the 32nd International Electric Propulsion Conference on Recirculating Liquid Nitrogen System for Operation of Cryogenic Pumps*, Hamburg, Germany, September 2011.
- ¹⁶I. Glassman, in *Combustion*, 2nd ed. (Academic, 1987), pp. 152–153.